International Journal of Nanomedicine

Dovepress
open access to scientific and medical research

Open Access Full Text Article

ORIGINAL RESEARCH

Dual Delivery of Tetramethylpyrazine and miR-194-5p Using Soft Mesoporous Organosilica Nanoparticles for Acute Lung Injury Therapy

Simin Min[1,2], Weiting Tao[1], Yuchen Miao[3], Yan Li[4], Tianyu Wu[5], Xiaoyu He[6], Yijing Zhang[7], Bangye Liu[7], Zixin Meng[7], Ke Han[1], Saisai Liu[1], Li Li[1], Jie Chen[1], Shidi Zhao[1], Junjie Zhang[3], Xiaonan Zhang[1]

[1]Bengbu Medical College Key Laboratory of Cardiovascular and Cerebrovascular Diseases, Bengbu Medical College, Bengbu, Anhui, 233030, People's Republic of China; [2]Suzhou Hospital of Anhui Medical University, Suzhou, Anhui, 234000, People's Republic of China; [3]Department of Chemistry, Bengbu Medical College, Bengbu, Anhui, 233030, People's Republic of China; [4]School of Medicine and Health Engineering, Changzhou University, Changzhou, Jiangsu, 213164, People's Republic of China; [5]School of Public Health, Bengbu Medical College, Bengbu, Anhui, 233030, People's Republic of China; [6]Department of Rheumatology and Immunology, The First Affiliated Hospital of Bengbu Medical College, Bengbu, Anhui, 233030, People's Republic of China; [7]School of Clinical Medicine, Bengbu Medical College, Bengbu, Anhui, 233030, People's Republic of China

Correspondence: Xiaonan Zhang, Department of Pathophysiology, Bengbu Medical College, 2600 Donghai Avinue, Longzihu District, Bengbu, Anhui, People's Republic of China, Tel +86-13609827842, Fax +86-552-3175283, Email zhangxn@bbmc.edu.cn; Junjie Zhang, Department of Chemistry, Bengbu Medical College, 2600 Donghai Avinue, Longzihu District, Bengbu, Anhui, People's Republic of China, Tel +86-16655208659, Fax +86-552-3175257, Email zhangjj@bbmc.edu.cn

Background: The respiratory system is intensely damaged by acute lung injury (ALI). The anti-inflammatory effects of tetramethylpyrazine (TMP) against ALI have been confirmed, but it exhibits a short half-life. miR-194-5p could directly target Rac1, but the internalization rate of miRNA cells was low.

Purpose: To explore the potential of the soft mesoporous organic silica nanoplatform (NPs) as carriers for delivery of TMP and miR-194-5p through the tail vein.

Methods: NPs@TMP and NPs@PEI@miR-194-5p were added to the HUVEC cell-lines, in vitro, to observe the cell uptake and cytotoxic effects. In vivo experiments were conducted by injecting fluorescently labeled NPs through the tail vein and tracking distribution. Therapeutic and toxic side-effects were analyzed systemically.

Results: In vitro study exhibited that NPs have no toxic effect on HUVECs within the experimental parameters and have excellent cellular uptake. The IVIS Spectrum Imaging System shows that NPs accumulate mainly in the lungs. NPs@TMP treatment can improved oxidative stress and inflammation levels in ALI mice and inhibited the TLR4/NLRP3/caspase 1 pathway. NPs@PEI@miR-194-5p can inhibit the Rac1/ZO-1/occludin pathway and improved endothelial cell permeability in ALI mice. The co-treatment of NPs@TMP and NPs@PEI@miR-194-5p can significantly improved the survival rates of the mice, reduced pulmonary capillary permeability and improved pathological injury in ALI mice.

Innovation: This study combined traditional Chinese medicine, bioinformatics, cellular molecular biology and nanobiomedicine to study the pathogenesis and treatment of ALI. The rate of cellular internalization was improved by changing the shape and hardness of nanoparticles. NPs@TMP and NPs@PEI@miR-194-5p combined application can significantly improve the survival condition and pathological injury of mice.

Conclusion: NPs loaded with TMP and miR-194-5p showed a greater therapeutic effect in ALI mice.

Keywords: NPs@TMP, NPs@PEI@miR-194-5p, tight junction, pulmonary capillary, endothelial cells, inflammation, acute lung injury

Introduction

Acute lung injury (ALI) is a serious inflammatory disease.[1] If ALI is not promptly treated, it will develop into a more serious form of acute respiratory distress syndrome (ARDS). The treatment of ALI is not definitive. Although mechanical ventilation is effective for treating ALI and ARDS, improper ventilation can cause lung damage. There is a great deal of clinical significance to seeking effective treatment strategies for ALI.

Received: 22 May 2023
Accepted: 27 October 2023
Published: 8 November 2023

Graphical Abstract

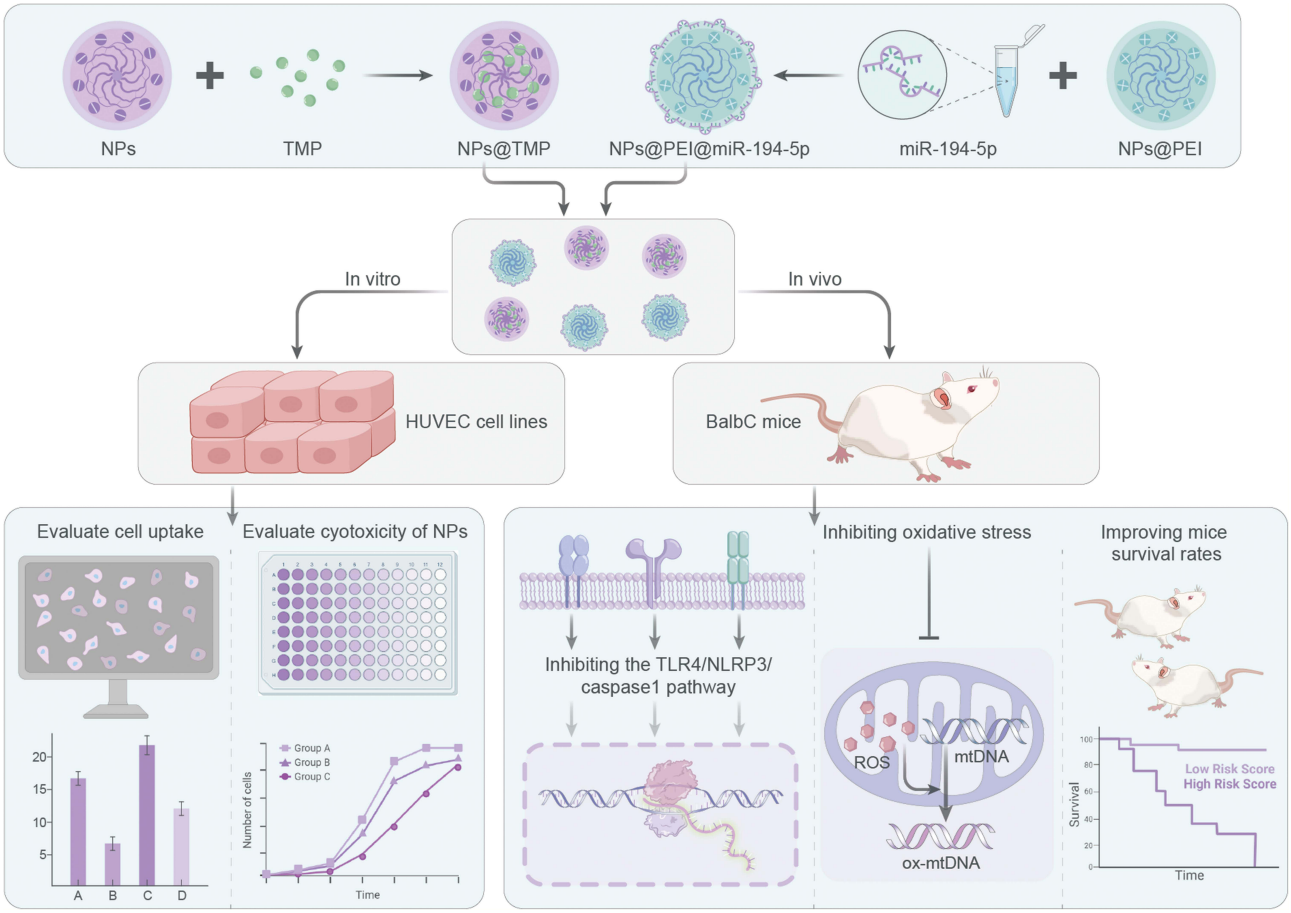

A series of pathological damages occur during ALI.[2,3] Uncontrolled inflammation can damage cells, tissues, and organs, as well as cause changes in the structure and function of the lungs, leading to severe respiratory failure.[4,5] As ALI develops, cellular permeability increases in the lungs, and the endothelial cell barrier is critical in maintaining lung permeability.[6] Many studies have confirmed that pulmonary endothelial cell dysfunction is a key part of the pathogenesis of ALI. Tight junctions (TJ), as the apical intercellular junction complex, inhibit solute and water flow through intercellular space (called the "gate" or "barrier" function). TJ also play a role in signal transduction.[7–9] Further, TJ are involved in the tight juxtaposition of transmembrane proteins between cells. Zonula occludens-1 (ZO-1) is closely related to scaffold protein and connects TJ transmembrane proteins such as claudins, junction adhesion molecules, and blocking proteins to the actin cytoskeleton. ZO-1 and α, β, together with p120 catenin, anchors transmembrane proteins to the actin cytoskeleton and connects TJ to adhesive junctions.[10] Ras-related C3 botulinum toxin substrate 1 (Rac1) is necessary to maintain cell adhesion and TJ. The increased activity of Rac1 promotes actin cytoskeleton remodeling and cell contraction, consequently reducing ZO-1 expression and resulting in the dysfunction of the endothelial barrier.[9,11] With the further development of ALI, monocytes and neutrophils are recruited from capillaries and the bone marrow to the inflammatory tissues, releasing proinflammatory cytokines and activating immune responses.

When neutrophils are activated,[12,13] they release a variety of toxic mediators, including reactive oxygen species (ROS) and myeloperoxidase (MPO), which are implicated in killing and degrading pathogens.[14] The release of a toxic medium cannot clear the pathogens in time, so neutrophils will continue to emit ROS, causing an increase in ROS in inflammatory lung tissue. As a result of high ROS levels, polyunsaturated fatty acids (PUFAs) within the biofilm are

peroxidized, and lipid hydroperoxide decomposition products are formed.[1] In the body, malondialdehyde (MDA) represents the degree of lipid peroxidation by reflecting cell damage, so it can reflect the degree of lipid peroxidation.[15,16] In addition, activation of Superoxide Dismutase (SOD) indirectly measures the body's ability to eliminate free radicals created by oxygen.[17,18] Therefore, ROS level reduction and improvement of the endothelial cell barrier function can alleviate lung permeability and inflammation.

NPs will preferentially accumulate in the lung given its vascular nature, hypertonicity, and retention capacity.[19] HMONs can easily enter human breast cancer MCF-7 cells by changing its morphological from sphere to ellipse, and this change lead to a 26-fold increase in cell uptake. HMONs are prone to surface modification by peptides or other functional groups. Additionally,[20] they have porous structures that enhance drug loading and release performance and thereby prevent short-term side effects caused by the high local concentrations of drugs and adverse reactions when administered alone.[21] With regard to ALI, NPs may be a suitable drug carrier because they accumulate in the lungs and inflammatory sites.[22] TMP is an effective antioxidant drug with a short half-life, low drug accumulation at the injured site, and causes some adverse reactions when used throughout the body.[23] In LPS-induced ALI, tetramethylpyrazine (TMP) provides protection through anti-inflammatory, anti-apoptosis effects. Therefore, NPs loaded with TMP has a bright prospect in treating ALI. Here, we prove that NPs@TMP has high anti-inflammatory and antioxidant effects in an ALI mouse model while minimizing unexpected side effects. In addition, currently synthesized naked miRNAs are unstable in sera rich in nucleases and are readily degraded, so developing an effective delivery system that can stably transport miRNAs remains challenging. As a nonviral delivery system, the soft mesoporous organic silica NP provides versatile platforms for exogenous microRNA expression in vivo. Differential expression of miR-194-5p in lung tissue of ALI mice. The present study identified Rac1 as a target of miR-194-5p. Rac1 is a subfamily of Rho small GTPases and modulates actin cytoskeleton-junctional protein interactions to regulate endothelial barrier function. These results demonstrate the potential of mesoporous silica nanoparticles (MSN) in developing new therapeutic strategies for ALI and other respiratory diseases.

Materials and Methods

Materials

TMP was obtained from the National Institute for the Control of Pharmaceutical & Biological Products (Beijing, China). LPS were purchased from Sigma-Aldrich (Saint Louis, USA). miR-194-5p was obtained from the Hanheng Biotechnology Company (Shanghai, China). This work employed the following resources: Cetyltrimethylammonium bromide (CTAB), bis-(triethoxysilyl) ethane (BTSE), 1.4-Bis(triethoxysilyl)benzene (BTSB), bis[3-(triethoxysilyl)propyl] tetrasulfide (TETS), Tetraethyoxysilane (TEOS) from Macklin; RBC lysis solution (Solaibao, China); ROS assay kit, BCA protein assay kit, and Cell Counting Kit-8 (CCK-8, Biyuntian, China); ELISA kit for IL-6, TNF-α, IL-1β, and MPO (Jingmei Biotechnology Co., Ltd., China). The primary antibodies were as follows: TLR4, NLRP3, caspase 1, Rac1, ZO-1, and occludin from Abcam and GAPDH (AbClone); Total RNA Extraction Reagent (NUOWEIZAN, Nanjing, China), all-in-One miRNA RT-qPCR (GeneCopoeia, USA), MDA and SOD assay kit (Jiancheng, Nanjing, China); and DAPI (Sigma-Aldrich) were also employed in this work.

Synthesis of HMONs

At 35°C, the 0.48 g of CTAB was dissolved in 3 mL of ammonia, 90 mL of anhydrous ethanol, and 375 mL of deionized water for 30 min. Then, the mixture of 0.375 mL of TEOS, 1.2 mL of BTSE, 0.3 mL of TETS, and 0.3 mL BTSB was added to the above mixture. The resulting mixture was allowed to react for 24 h, centrifuged, and washed with anhydrous ethanol for 3 times to obtain organo-oxide/CTAB nanocomposite spheres. Sodium hydroxide solution (0.48 M) was then added to 25 mg of nanocomposite balls and placed in a shaker at room temperature for 30 minutes. We then centrifuged and washed the product three times with deionized water. In the final step, the product was added to a solution of concentrated hydrochloric acid and ethanol and stirred at 60°C for 3 h. The operation was repeated 3 times to obtain the final HMONs.

Synthesis of HMONs-PEG-Cy5.5 (NPs)

The reduced HMONs were obtained by adding 0.65 mg of HMONs to a mixture of 0.3 mL of deionized water, 1.1 mL of dioxane, 40 μL of concentrated hydrochloric acid, and 0.1 g of triphenylphosphine at 40°C for 2 h and then washing the mixture for three times with deionized water. Then, 12 mg of reduced HMONs was mixed with 1.2 mL of N, N-dimethylformamide and 3.24 mg of PEG-MAL for 12 h at room temperature, followed by the addition of 1.2 mg of Cy5.5-MAL for 12 h at room temperature to obtain HMONs-PEG-Cy5.5. In cases where the emission wavelength of Cy5.5's near-infrared fluorescent dye was beyond the range of vision, the appearance of Cy5.5's pseudocolor as red was assigned.

Synthesis of NPs@TMP

Subsequently, 10 mg of NPs was dispersed in a PBS solution of 5 mL of TMP (1 mg/mL) and oscillated for 12 h in the dark. The product was then centrifuged and washed three times with deionized water to obtain NPs@TMP. The supernatant and washing solution were collected and the loading rate was calculated.

Synthesis of NPs@PEI@miR-194-5p

After dispersing 1 mg of NPs in 1 mL water, polyethylenimine (PEI) aqueous solution was added to the mixture (the mass ratio of PEI to NPs was 2:0.5), and ultrasonic dispersion was performed for 30 min. The product was then centrifuged and washed thrice in ethanol and water. The product was dispersed in 125 μL miR-194-5p solution (20 μM) and incubated for 20 min at room temperature. Consequently, we obtained NPs@PEI@miR-194-5p.

Cell Culture in vitro

HUVECs were obtained from ATCC (ATCC, USA). HUVECs were cultured in high-glucose DMEM (Gibco, USA) containing 10% FBS (Gibco, USA), 1% penicillin-streptomycin (Gibco, USA), and 0.5% glutamine (Gibco, USA). Incubator settings of 37°C and 5% CO_2 were used to incubate the cells.

Cell Viability Assays

In HUVEC cells, NPs were tested for cytotoxicity using the Cell Counting Kit-8 (CCK-8). Cells were seeded into 96 well plates overnight at a density of 1×10^4 cells/well. In the following 12 hours, the medium was replaced with 100 μL of medium containing NPs in different concentrations (0, 100, 200, 300, 400, and 500 μg/mL). The plates were incubated for 2 hours after the addition of the CCK-8 solution to each well following 24 h of incubation. An absorbance measurement was then performed on a microplate reader at 450 nm.

Animal Experiments

All animal experiments in this work were approved by the Bengbu medical college's ethics (the registration number: 2021–192, 25 June 2021). The use of experimental animals adhered to the 3R principles. Pathogen free, 6–8-week-old male BalbC mice were obtained from the Changzhou Card Vince Laboratory Animal Co., Ltd (Certification number: SCXK 2021–0013; Changzhou, China). We used a pseudo randomization method to allocate the mice. A mouse ALI model was established by treating BalbC mice with LPS as described previously. We divided the BalbC mice evenly and randomly into nine groups: control, LPS, NPs, free TMP, Dex, NPs@TMP, NPs@PEI, NPs@PEI@miR-194-5p, and NPs@TMP+NPs@PEI@miR-194-5p. Twelve hours before the first administered intraperitoneally (i.p.) and second intratracheally (i.t) LPS administration, injections of 100μL of PBS were given intravenously (i.v.) to the mice, 100 μL of NPs (PBS suspensions, 5 mg/mL), free TMP (PBS suspensions, 10 mg/mL), and Dex (DMSO-dissolved, 0.4 mg/kg), NPs@TMP (PBS suspensions, 5 mg/mL, equal to 10 mg/kg of free TMP), respectively. Twelve hours before the first i.p. LPS administration, the mice were i.v. administered with NPs@PEI@miR-194-5p (suspensions in PBS, equal to 5 nmol of miR-194-5p) and equivalent concentrations of NPs@PEI. PBS-treated mice served as negative controls. The animals were sacrificed 24 hours after LPS treatment to collect the lung tissues and BALF. During the 7-day experiment, day-to-day monitoring of the survival rate was conducted.

NPs Distribution in vivo

An ALI model was created and then NPs (100 μL, 5 mg/mL) were injected i.v. into the tails of mice. PBS was injected i. v. into control mice. After NP administration, the mice were anesthetized and sacrificed at 8, 12, and 24 hours, and an IVIS Spectrum In Vivo Imaging System was used to image the heart, liver, spleen, lung, and kidney.

Wet/Dry Ratios of Lung

After 24 h following LPS treatment (i.t), the mice were anesthetized and sacrificed. Dissection of the right lung was followed by collection of the lung and recording of the wet weight. To calculate the dry weight, the lung was baked at 70 °C for 72 hours. Calculating the lung wet/dry ratio (W/D) effectively assessed lung edema.

Bronchoalveolar Lavage Fluid Collection and Analysis

The Mice were anesthetized with isoflurane and sacrificed by cervical dislocation. The lungs were exposed and slowly injected with precooled PBS. Bronchoalveolar lavage fluid (BALF) was collected after the lungs were lavaged twice with 0.8 mL of PBS. At 4 °C, five minutes of centrifugation at 1200 rpm/min was applied to BALF samples. RBCs were lysed with RBC lysis solution for 15 minutes. Using a standard hemocytometer, BALF total leukocyte counts were determined, and total protein concentrations in BALF were ascertained with BCA protein assay kits. According to the manufacturer's instructions, ELISA kits were employed to measure the TNF-α, IL-1β, IL-6, and MPO levels in the BALF.

Western Blot

The total protein from lung tissue was extracted with RIPA lysate buffer. Protein lysates (20 μg) from each sample were mixed in SDS-loading buffers and boiled at 100°C for 5 min. The mixture was run on 10%–12.5% SDS-PAGE gels and then transferred to a PVDF membrane. Then, 5% fat-free skimmed milk was used to block PVDF membranes for 2 h at room temperature, Primary antibodies were incubated overnight at 4 °C, including TLR4 (1:1000), NLRP3 (1:1000), caspase 1 (1:1000), Rac1 (1:1000), ZO-1 (1:1000), occludin (1:1000), and GAPDH (1:10000). After washing, the membranes were incubated for 1 h at room temperature with secondary horseradish peroxidase antibodies and visualized using the chemiluminescence system.

Validation Test of Quantitative Real Time PCR

Total RNA was extracted using the Total RNA Extraction Reagent. miRNA qPCR was performed using All-in-One miRNA RT-qPCR.

Flow Cytometry

HUVEC cells were seeded in six-well plates for flow cytometric analysis. After 12 h, Cy5.5-labeled NPs were added to the six-well plates. Cells were harvested at 8, 12, and 24 h. Cellular uptake for Cy5.5-labeled NPs was analyzed by flow cytometry. Using the ROS Assay Kit, cell suspensions in BALF were stained. DCFH-DA was used as a fluorescent probe according to the instructions and by using a CytoFLEX flow cytometer. An analysis of the data was conducted with the FlowJo Oxidative Stress software (FlowJo 10.0, USA).

Oxidative Stress

Malondialdehyde (MDA) is generated due to oxidative stress, when fatty acids within cells are oxidized. When unsaturated fatty acids react with ROS, MDA is formed. MDA determination often coincides with a SOD determination. SOD activity indirectly indicates the body's oxygen free radical scavenging capacity, and cell damage from free radicals is indirectly reflected by MDA. In an ice water bath, lung tissue homogenates were prepared at a ratio of 1:9 lung tissue to normal saline. After centrifugation at 3000 rpm/min for 10 minutes at 4°C, the supernatant was collected to obtain 10% homogenate supernatant for use, and the protein concentration of the supernatant was detected with a BCA Kit (Biyuntian, China). The supernatant was obtained and detected following the MDA and SOD activity detection assay kit instructions. The absorbance values were taken at 532 nm using a U-2600 UV–Vis spectrophotometer.

Systemic Inflammation and Oxidative Stress

To quantify serum cytokines, peripheral blood was collected from the posterior orbital venous plexus of mice and stored for 2 h at room temperature. After centrifugation of the blood at 4 °C, the serum was obtained. According to the ELISA, MDA and SOD assay kits manufacturer's instructions, TNF-α, IL-1β, IL-6, MDA, and SOD were measured, respectively.

Cellular Uptake of NPs in vitro

To investigate the NP uptake of HUVEC, confocal laser microscopy was applied. We plated HUVEC cells at a density of 3×10^5 cells per well in 6-well plates for 12 hours, and the cells were brought to the defined confluence. Subsequently, 1 mL of fresh medium containing 100 mg/mL NPs was added, and the cells were incubated for 8, 12, and 24 hours. Then, the medium was discarded and the cells were washed thrice with PBS, fixed for 15 min with 4% paraformaldehyde, and washed thrice with PBS after DAPI staining of the nuclei. Using confocal laser endomicroscopy, the cell images were scanned.

Lung Histology and Lung Injury Score

The lung tissue of mice was collected 24 h after intratracheal instillation of LPS. 4% paraformaldehyde was used to fix the removed lung tissues. After dehydration and paraffin embedding, all tissues were cut into 5-μm thin sections. The lung injury score was determined by a pathologist blinded to the experimental groups. The following parameters were considered for each image to score: (A) inflammatory infiltration, (B) alveolar edema, (C) interstitial edema, and (D) hemorrhage. The HE scores were denoted as follows (Wang et al, 2012): 0 = no damage, 1=mild damage, 2=moderate damage, and 3=extreme damage.

Molecular Docking

The crystal structure of the human TLR4-MD-2 complex (PDB code: 2Z65) was downloaded from Protein Data Bank (PDB) (https://www.rcsb.org/). TMP downloaded from https://pubchem.ncbi.nlm.nih.gov/. Autodock was used to analyze the combined energy of TMP and TLR4.

Statistical Analysis

All results are expressed as mean value ± standard deviation (mean ± SD) unless stated otherwise. A Student's *t*-test was used to determine whether two groups differed significantly, and the significance of differences among multiple groups was determined by one-way analysis of variance. The Kaplan–Meier survival analysis was performed with the log-rank method. A P value of less than 0.05 ($P<0.05$) indicated statistical significance.

Results and Discussion

Preparation and Characterization of NPs and NPs@PEI

In this study, we synthesized deformable hollow mesoporous organosilica NPs (HMONs) by a preferential etching approach. HMONs were selected as the scaffolds for the fabrication of nanodevices. The external surface was functionalized with PEG (HMONs-PEG), and the surface of HMONs-PEG was modified with near-infrared dye Cy5.5 to synthesize HMONs-PEG@Cy5.5 (NPs). NPs were functionalized with polyethylenimine (PEI) to synthesize NPs@PEI. Then, the pores were loaded with TMP (NPs@TMP), and the miR-194-5p (NPs@PEI@miR-194-5p) was adsorbed on the surface of NPs@PEI through electrostatic attraction. In ALI mice models, the NPs are expected to deliver their cargo to the inflamed lungs. Scheme 1 illustrates how the nanodevices are structured.

The prepared NPs were characterized by TEM, zeta potential, and FTIR. According to TEM images, HMONs showed a cross-wrinkled morphology with collapsed hollow nanocapsules (Figure 1A and B indicate that HMONs had a negative zeta potential value (−17±1 mV). After PEI and functionalization, the zeta potential of HMONs-PEG (−25±4 mV) and NPs (−34±1 mV) changed to positive (NPs@PEI, 36±2 mV). The results (Figure 1C) showed that the absorption peaks at 1411 cm^{-1} was the peaks of the $–CH_2–CH_2–$ group; The peaks at 1158 cm^{-1} were attributed to C-H bending vibration of the benzenoid ring; the characteristic vibrational band of C–S group appeared at 686 cm^{-1}; 900–1300 cm^{-1} is the

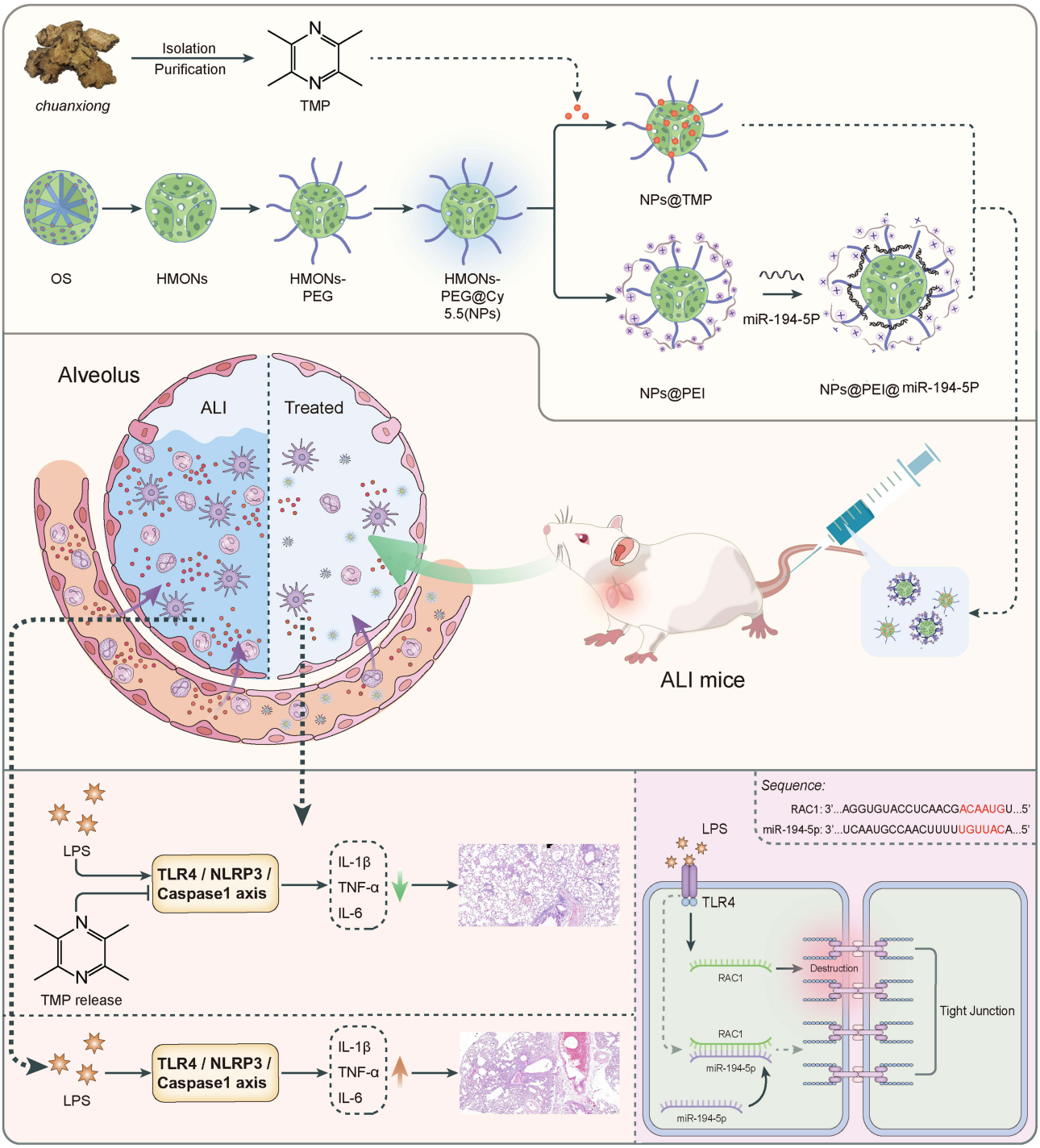

Scheme 1 NPs loaded with Dex and miR-194-5p are used to demonstrate in vivo therapy for ALI mice. The intravenously injected NPs@PEI and NPs@PEI@miR-194-5p accumulate in lung, and release drug-triggered, resulting in decreased immune cell infiltration and cytokines, partly restored the impaired epithelial tight junction, and thereby reduced lung injury.

vibration peak of Si-O-Si; These results indicating that ethane, phenyl, and thioether groups have been successfully doped into the HMONs skeleton. In addition, the appearance of peak at 1630 cm^{-1} corresponded to the stretching vibration of C=N from TMP.

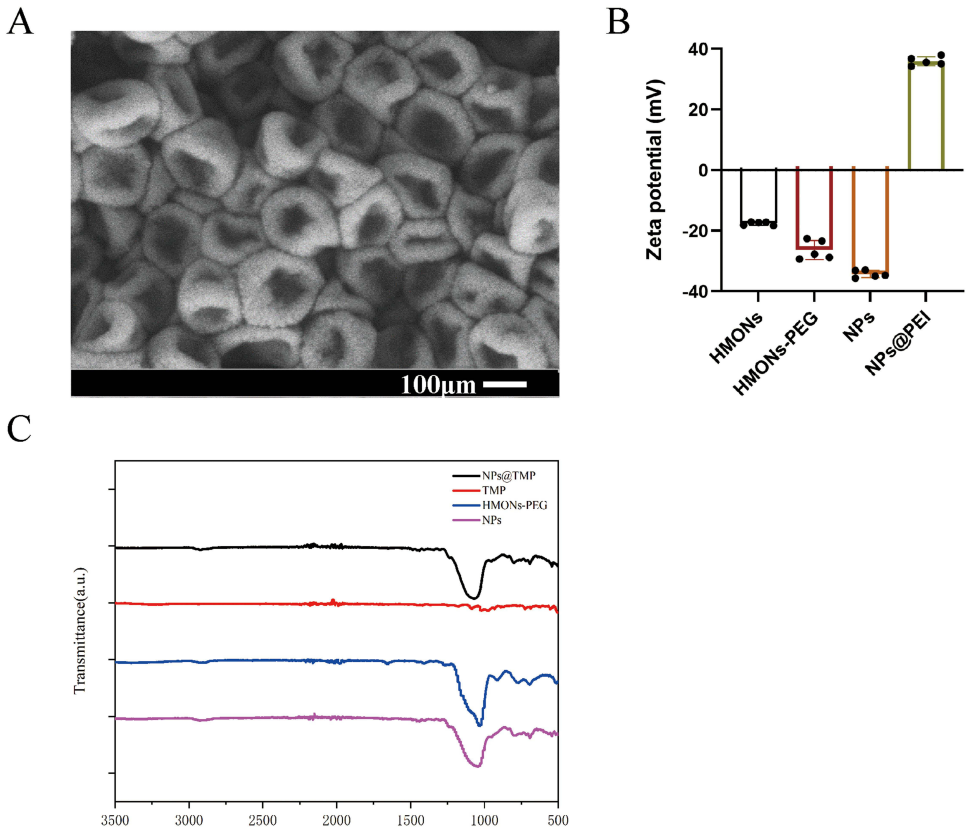

Figure 1 The characteristics of NPs. (**A**) SEM images of HMONs, scale bars=100 μm. (**B**) Zeta potential of HMONs, HMONs-PEG, NPs and NPs@PEI. A change in the zeta potential from negative to positive was observed when NPs was combined with PEI. (**C**) Fourier transform infrared spectrometer spectra of HMONs-PEG, NPs, TMP, and NPs@TMP.

Cytotoxicity and Cellular Uptake of NPs

HMONs and HMONs-PEG@Cy5.5 (NPs) did not appear to be toxic to HUVEC cells within the investigation range of 0–500 μg/mL in the CCK-8 assay (Figure 2A and B). To investigate the cellular uptake of NPs into HUVECs, NPs labeled with Cy5.5 were used. By applying confocal laser scanning microscopy, we investigated HUVEC uptake qualitatively. The HUVECs were incubated with NPs for 8, 12, and 24 h. The confocal immunofluorescence microscopic images (Figure 2C) and flow cytometry analysis (Figure 2D) showed that the NPs began to internalize quickly at 8 h of co-incubation, and their amount gradually increased.

NP Distribution and Safety Evaluation

To examine NP distribution in vivo, an immunofluorescence experiment was performed on frozen sections of the tissues (heart, liver, spleen, lung, and kidney) 24 h post-injection. The immunofluorescence analysis results showed that apparent aggregation of NPs in lung tissue (Figure 3A). Next, we used IVIS Spectrum Imaging System for further validation of the in vivo NP distribution in tissue. The results also showed that the most aggregation occurred in the lung, and that NP aggregation increased over time (Figure 3B). The toxicity of NPs was assessed by HE staining, and Figure 3C reveals that NP treatments did not obviously cause pathological injury in the main organs. No significant abnormalities were found in blood routine tests, which mainly comprised red blood cell specific volume (HCT), white blood cell (WBC), hemoglobin (HGB), platelets (PLT), and RBC (Figure S1).

ROS Inhibition Effect of NPs@TMP in vivo

At pH 7.4, TMP was released from NPs@TMP rapidly within the first two hours, and then slowly, reaching more than 20% after 48 hours (Figure S2). The overproduced ROS generates oxidative stress, contributing to cellular damage and

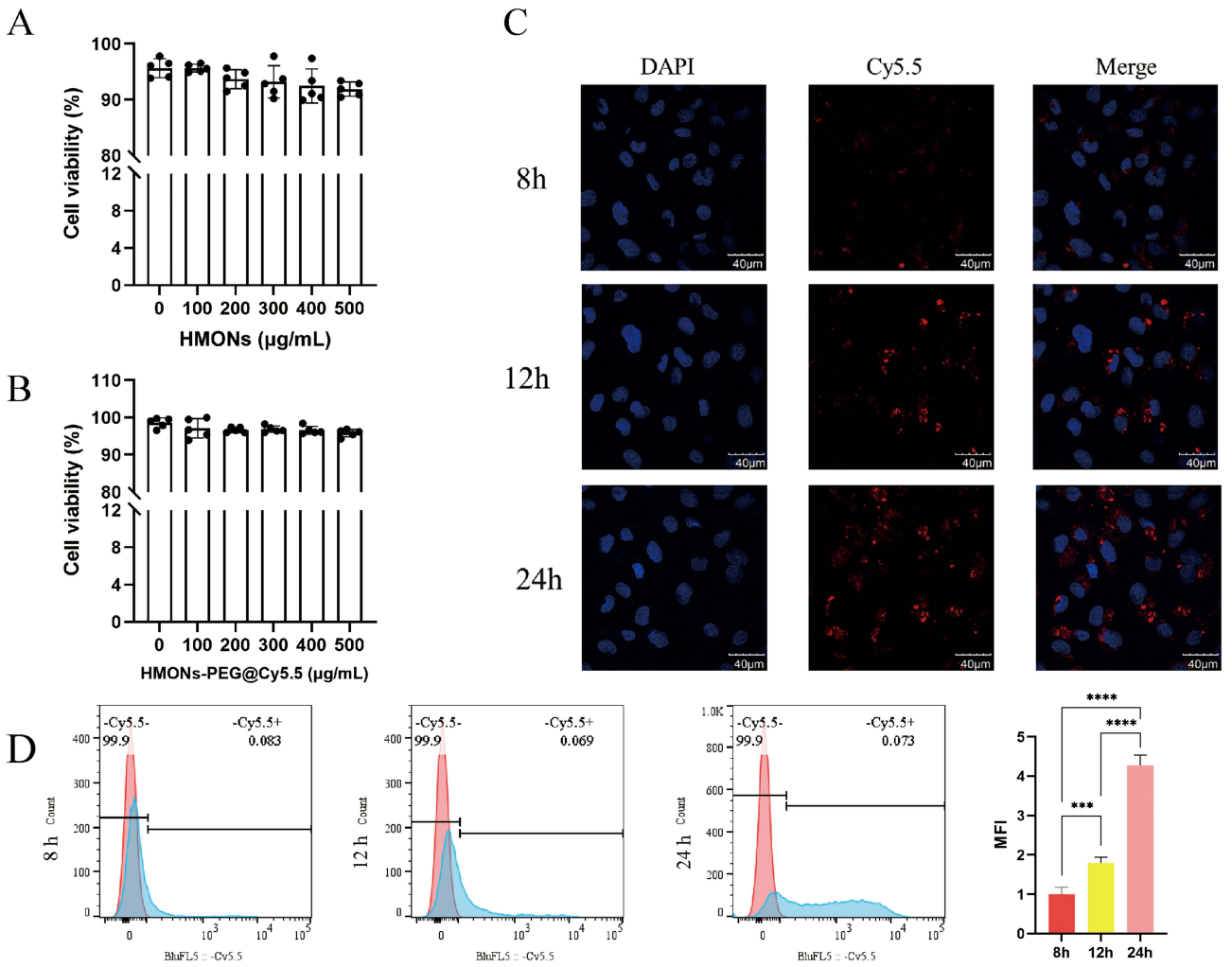

Figure 2 Relative cytotoxicity of NPs and NPs@TMP of different concentrations after being incubated with HUVEC cells for 24 h. Relative cytotoxicity of. (**A**) NPs and (**B**) NPs@TMP of different concentrations after being incubated with HUVEC cells for 24 h determined by CCK-8 assay. (**C**) The CLSM images were taken after various incubation times, and the NPs were stained with DAPI (blue) and the cell nuclei with Cy5.5 (red). Scale bar = 40 μm. (**D**) Internalization of Cy5.5-labeled NPs by HUVECs analyzed by flow cytometry and the calculated mean fluorescence intensity (MFI). ***p < 0.001, and ****p < 0.0001.

amplifying the inflammation process. The levels of ROS in the BALF were detected using flow cytometry. As shown in Figure 4A, LPS stimulation led to an increased ROS production. Given the intrinsic anti-inflammatory properties of Dex, it significantly inhibited ROS production. Thus, the positive control was Dex. By contrast, free TMP decreased ROS levels because of its ability to scavenge free radicals. However, the NPs@TMP had a more remarkable effect on inhibiting the ROS level (Figure 4A). The results are presented as mean fluorescence intensity (MFI) histograms (Figure 4B). As ALI progresses, overproduced ROS can oxidize proteins, lipids, and DNA. Therefore, evaluating the antioxidant capacity of NPs by assessing the amount of tissue oxidative damage is essential. The MPO enzyme promotes oxidative stress at sites of inflammation by producing free radicals. Nevertheless, excessive MPO causes tissue damage at inflammatory sites because of oxidative stress. After LPS stimulation, MPO expression increased significantly, indicating neutrophil infiltration. MPO activities of the BALF in the free TMP, DEX, and NPs@TMP treatment groups was significantly decreased, compared with that of LPS group (Figure 4C). MDA and SOD levels in the lung were also used as indicators of oxidative stress. LPS stimulation increased MDA levels and decreased SOD levels, but MDA levels significantly decreased and SOD levels increased with free TMP, DEX, and NPs@TMP treatment. (Figure 4D and E). These outcomes indicate that NPs@TMP has good antioxidative stress property.

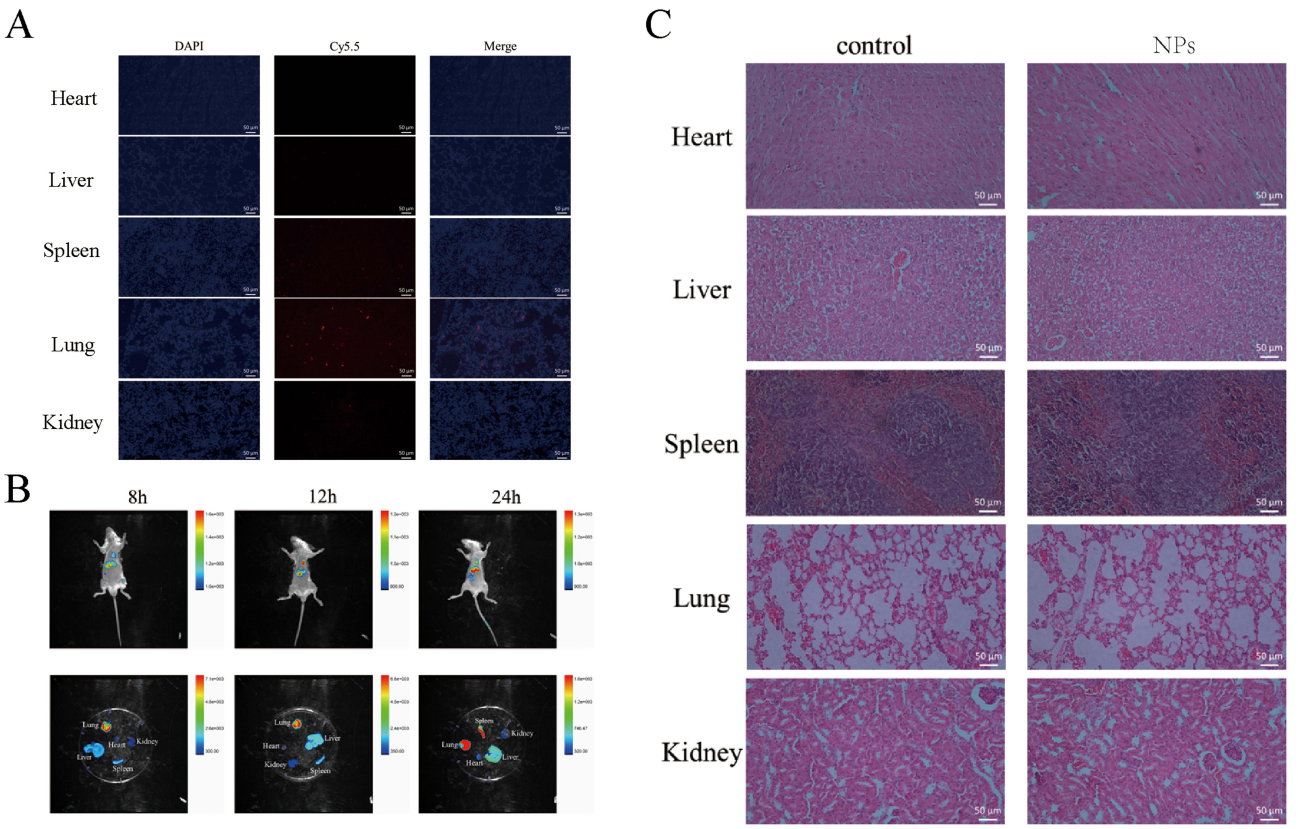

Figure 3 Distribution and safety evaluation of NPs in vivo. (**A**) Fluorescent images of various tissues, with the NPs labeled with Cy5.5 (red), and the cell nuclei stained with DAPI (blue). Scale bar = 50 μm. (**B**) The fluorescence intensity of NPs in different tissues observed by IVIS Spectrum Imaging System at various times after NPs (5 mg/mL) were injected into the tail vein of mice. (**C**) HE staining sections collected from the heart, liver, spleen, lung, and kidney of the control and HMONs@PEG@Cy5.5 groups. Scale bar = 50 μm.

Anti-Inflammation Efficacy of NPs@TMP in vivo

Molecular docking experiments was conducted to further explore the anti-inflammatory mechanism of TMP. The molecular docking results of TMP and TLR4 was shown in Figure 5A. The results indicated that TMP could interact with TLR4 through the amino acids TYR-72 and ILE-48 (Figure 5A). Compared with the control group, WB results confirmed that LPS treatment significantly increased TLR4, NLRP3, and caspase 1 protein levels, indicating that the TLR4/NLRP3/caspase 1 signaling pathway was activated (Figure 5B–D). The levels of TLR4, NLRP3, and caspase 1 protein expression were not significantly altered following NP treatment; however, these levels decreased with free TMP, DEX, and NPs@TMP treatment (Figure 5B–D). As part of the study, we tested whether NPs@TMP can modulate inflammatory responses. TMP is a potent anti-inflammatory and immunosuppressant that reduces the release of inflammatory factors. The levels of inflammatory factors were increased by treatment with LPS. To analyze the anti-inflammatory effect of NPs@TMP, mice with LPS-induced ALI were pretreated with free TMP, DEX, and NPs@TMP. The free TMP, DEX, and NPs@TMP significantly decreased the IL-6, TNF-α, IL-1β expression levels of BALF compared to the LPS group (Figure 5E–G). In addition, the BALF of mice significantly increased in protein concentration after exposure to LPS; by contrast, BALF protein concentration decreased significantly after treatment with NPs@TMP (Figure S3). These data indicate that LPS-induced an inflammatory response and increased vascular permeability in the mouse lungs, and NPs@TMP can inhibit inflammatory responses and vascular hyperpermeability.

NPs@PEI@miR-194-5p Improve Endothelium Barrier Function

The miR-194-5p expression was decreased in ALI mice, and the dual-luciferase reporter assay results showed that miR-194-5p targeted Rac1 (Figure 6A). In this study, the cell internalization performance of miR-194-5p was improved by

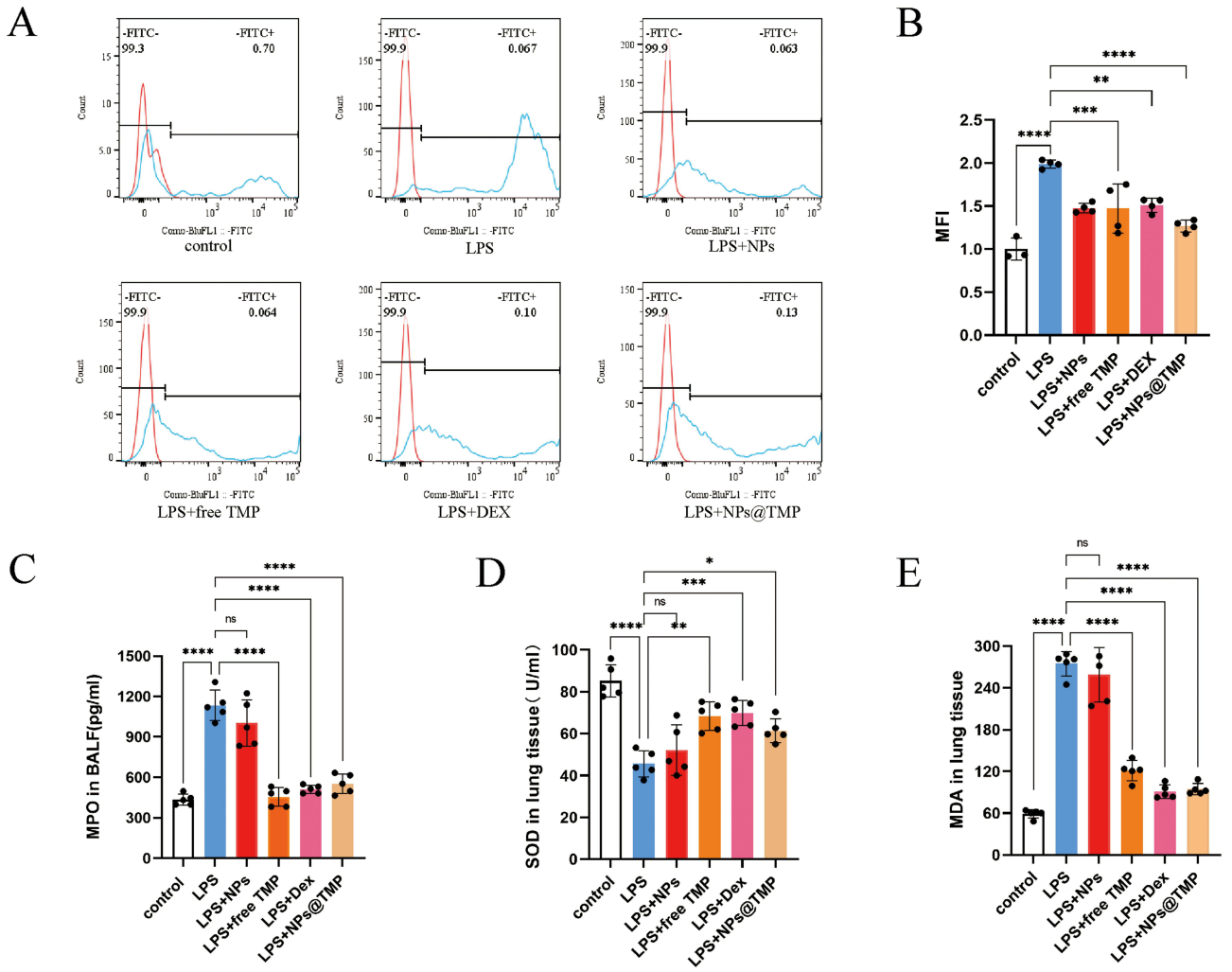

Figure 4 NPs@TMP antioxidant capacity in vivo. (**A**) Expression levels of ROS from the BALF analyzed by flow cytometry, and (**B**) the calculated MFI after the treatment. (**C**) Expression levels of MPO with different treatment groups in BALF. Quantification of (**D**) SOD and (**E**) MDA levels in lung tissue homogenates of ALI mice after various treatments. *P < 0.05,**p < 0.01, ***p < 0.001, and ****p < 0.0001. ns: no significant difference.

loading it into PEI-modified NPs. The HUVECs were incubated with NPs@PEI@miR-194-5p for 24 h, and the expression levels of miR-194-5p increased 4–5 times in HUVECs (Figure 6B) and 6–7 times in lung tissue (Figure 6C). Figure 6D indicates that the NPs@PEI@miR-194-5p treatment reduced LPS-induced Rac1 expression. Given that the function of endothelial barrier integrity depends on occludin's interactions with ZO-1 and its localization within the membrane, Western blot analysis of occludin and ZO-1 expression in the entire lung tissue protein lysate was conducted. No differences occurred between the LPS and LPS+NPs@PEI groups (Figure 6E and F). Remarkably, ZO-1 and occludin protein expression levels increased after treatment with NPs@PEI@miR-194-5p (Figure 6E and F).

NPs@TMP and NPs@PEI@miR-194-5p Combination Therapy for ALI Mice

Systemic inflammation, oxidative stress, and endothelial dysfunction are also serious during the onset and development of ALI. Therefore, we detected the expression levels of inflammatory factors SOD and MDA in serum, and Evans blue detected the permeability of pulmonary capillary endothelial cells. The expression levels of inflammatory factors (IL-6, TNF-α, and IL-1β), MPO, in serum were significantly reduced with NPs@TMP and NPs@PEI@miR-194-5p treatment compared to the LPS group (Figure 7A–D). Meanwhile, NPs@TMP therapy combined with NPs@PEI@miR-194-5p significantly attenuated the increased inflammatory factors (IL-6, TNF-α, and IL-1β), MPOin serum (Figure 7A–D). LPS stimulation decreased SOD levels and increased MDA levels, but SOD levels significantly increased and MDA levels decreased with NPs@TMP and

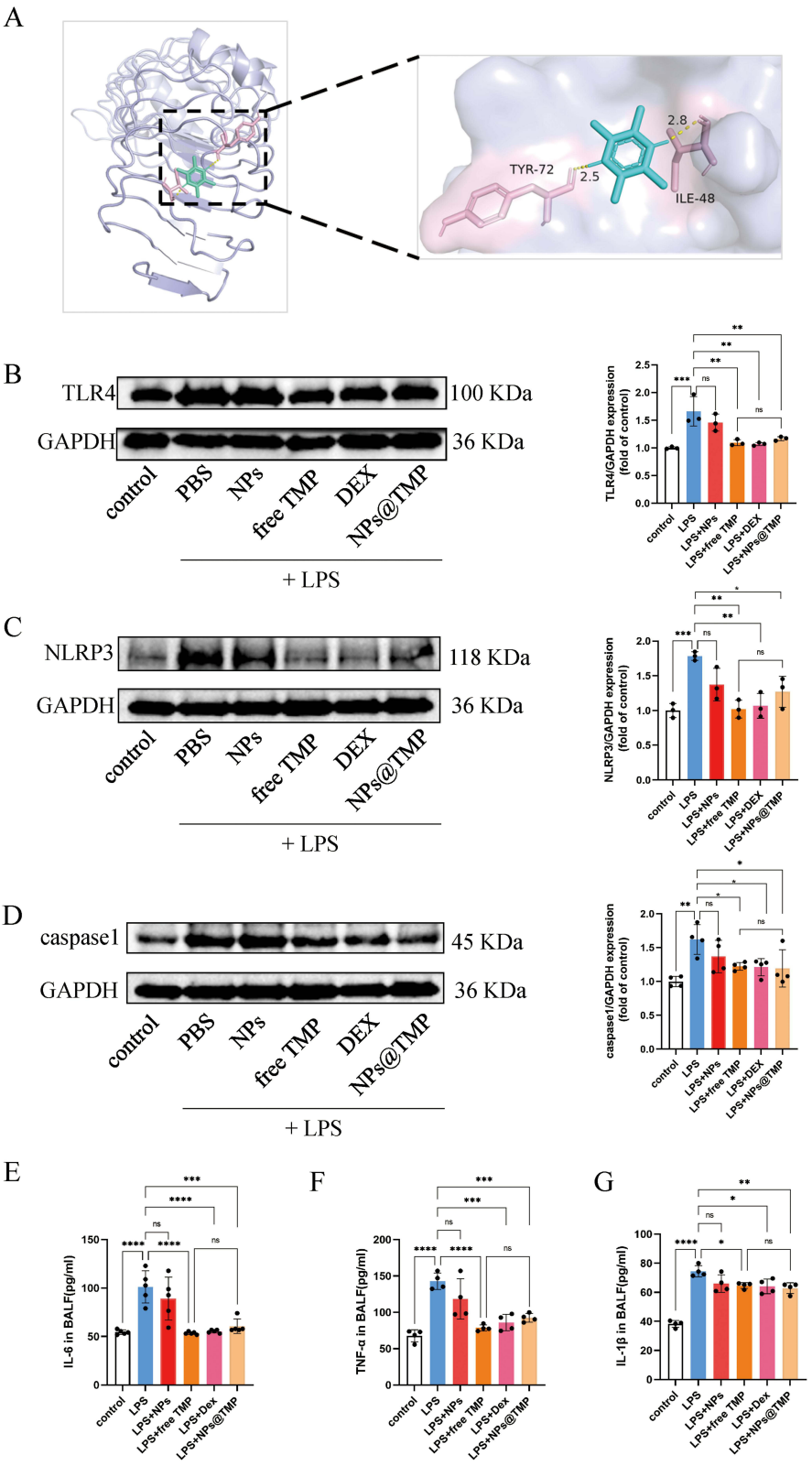

Figure 5 NPs@TMP anti-inflammatory and anti-apoptotic effects in vivo. (**A**) The molecular docking data of TMP on TLR4 dimer were analyzed by using Autodock software, showing ligand (green), TLR4 residues (pink), and hydrogen bonds (yellow lines). Western Blot experiment was conducted to further confirm that TMP targeted TLR4 proteins. The protein expressions of (**B**) TLR4, (**C**) NLRP3, and (**D**) caspase 1 in lung tissue by Western Blot. Quantification of (**E**) IL-6, (**F**) TNF-α, and (**G**) IL-1β levels in BALF of ALI mice after various treatments. *p < 0.05, **p < 0.01, ***p < 0.001, and ****p < 0.0001. ns: no significant difference.

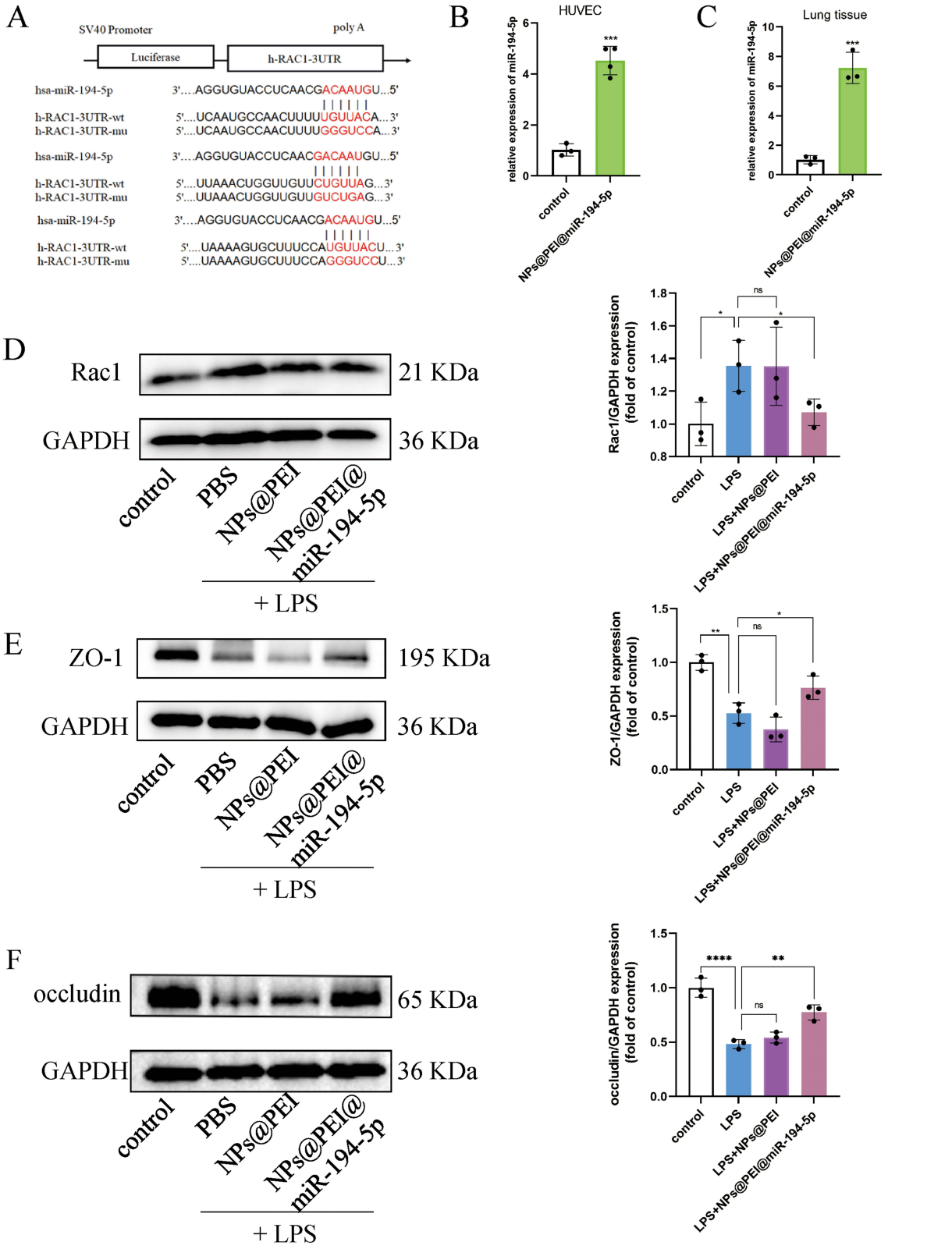

Figure 6 Improvement of endothelium barrier function by NPs@PEI@miR-194-5p. (**A**) Predicted miR-194-5p binding sites in the Rac1 3-UTR by Dual-luciferase reporter assay. (**B**) The transfected HUVECs and (**C**) lung tissues were harvested at 24 h post-transfection and after semiquantitative analysis of miR-194-5p expression level by qPCR 24. Western blot analysis of the expression of (**D**) Rac1, (**E**) ZO-1, and (**F**) occludin in lung tissues. *p < 0.05, **p < 0.01, ***p < 0.001, and ****p < 0.0001. ns: no significant difference.

https://doi.org/10.2147/IJN.S420802 DovePress

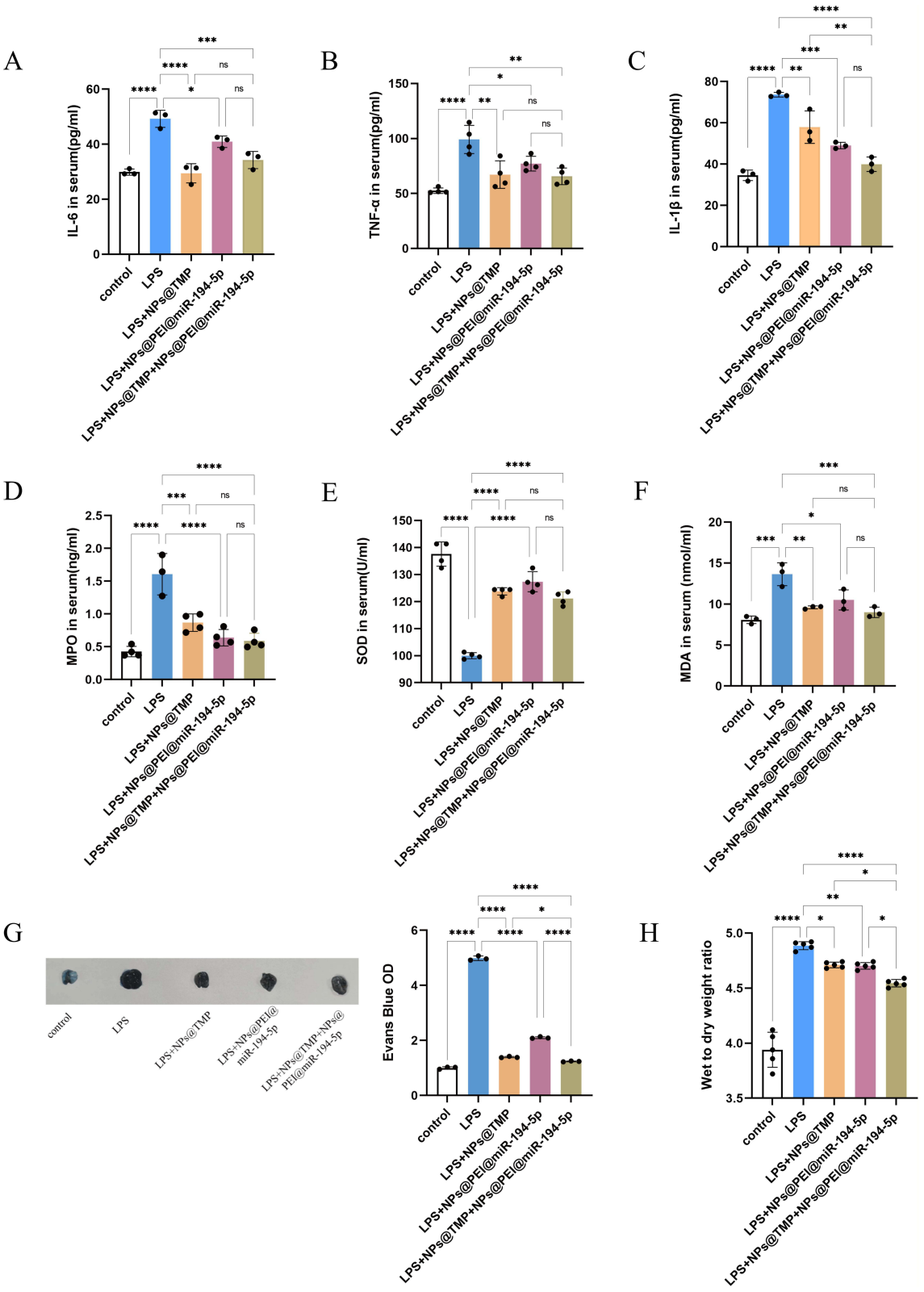

Figure 7 NPs@TMP and NPs@PEI@miR-194-5p combination therapy for mice. Quantification of (**A**) IL-6, (**B**) TNF-α, and (**C**) IL-1β levels in the serum of ALI mice after various treatments. (**D**) Expression level of serum MPO for different treatment groups. Quantification of (**E**) SOD and (**F**) MDA levels in the serum of ALI mice after various treatments. The mice were sacrificed two hours after the intravenous injections of Evans Blue. (**G**) Representative pictures of lung tissue and the quantitative analysis of Evans Blue leakage in lung tissue. (**H**) Various treatments for lung W/D ratios. *p < 0.05, **p < 0.01, ***p < 0.001, and ****p < 0.0001. ns: no significant difference.

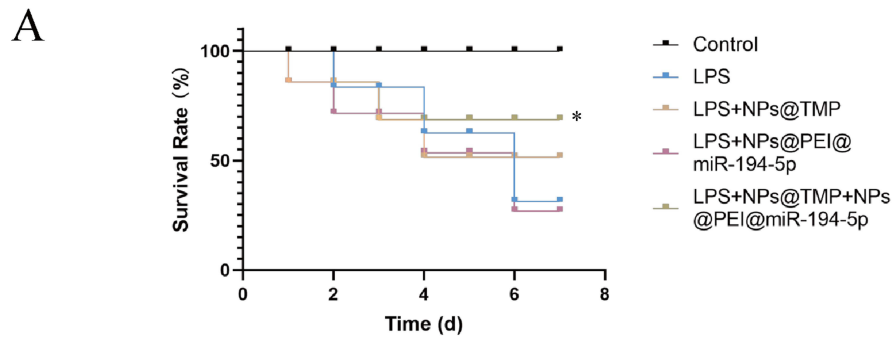

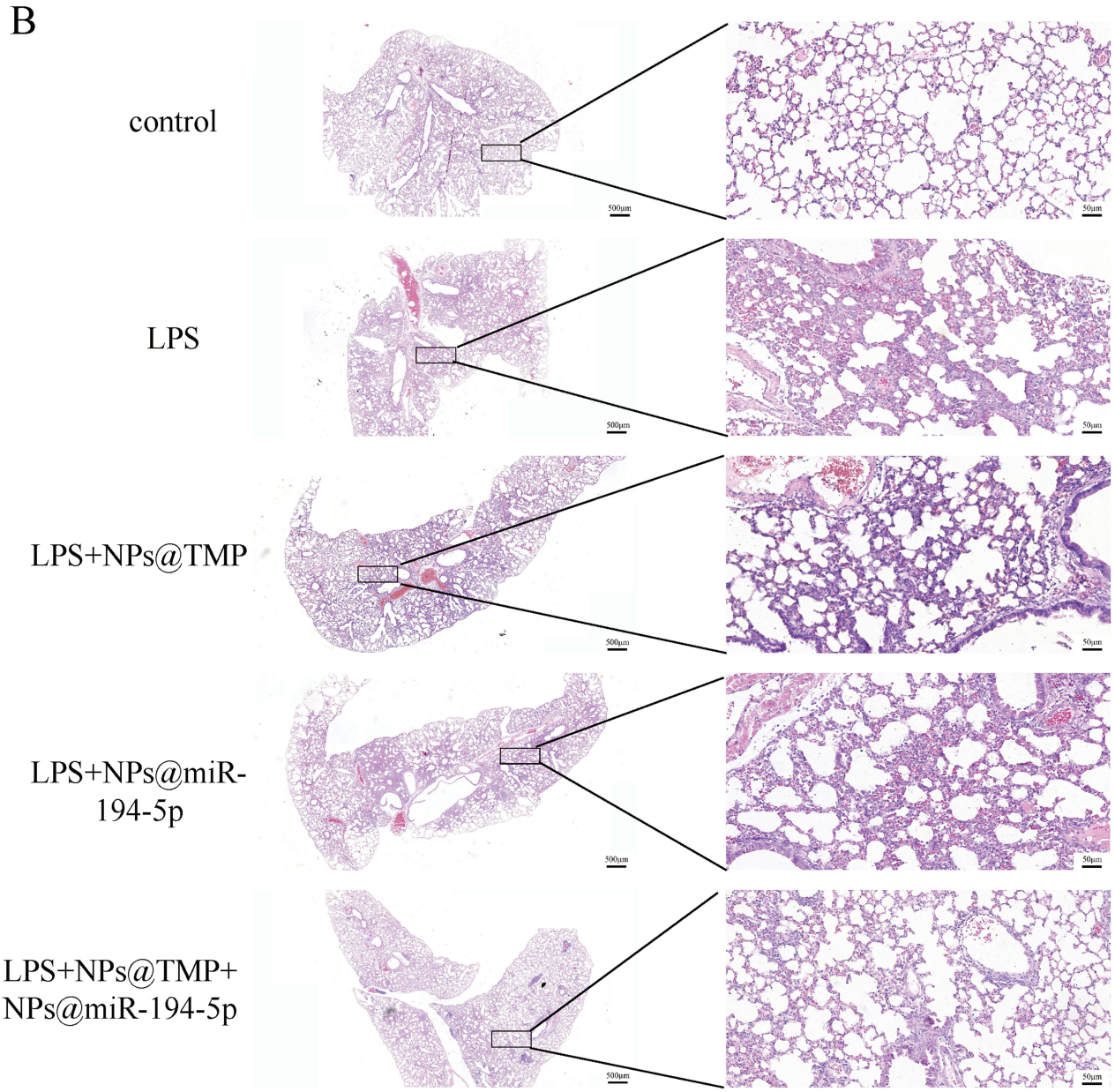

Figure 8 Combination treatment significantly increased overall survival and obviously improved the pathological injury. (**A**) The ALI model was established by intratracheally injecting LPS into BalbC mice. We injected different formulations intravenously into mice, and monitored their survival every 24 h for 7 days following LPS (4 mg/kg) administration. (**B**) HE images of ALI mice with the lung various treatments. *p < 0.05.

NPs@PEI@miR-194-5p treatment compared to the LPS group. (Figure 7E and F). Lung microvascular endothelial cell permeability in lung tissue was measured using the Evans blue and wet/dry ratio methods. Evans blue dye was injected into the tail vein 2 h before euthanasia, and the lungs were removed to detect Evans blue extravasation. The LPS group exhibited serious Evans blue extravasation. The combined treatment had superior effect relative to individual NPs@TMP or NPs@PEI@miR-194-5p treatment (Figure 7G). Similarly, mice treated with the combination therapy had a significant reduction in wet/dry weight ratios compared to control mice (Figure 7H). A combination of NPs@TMP and NPs@PEI@miR-194-5p therapy could prolong mouse survival time and increase survival rates (Figure 8A). In addition, HE staining results revealed that LPS treatment of mice induced lung pathological injury, and the co-treatment obviously improved the pathological injury (Figure 8B).

Conclusion

Given its vascularity, high permeability, and retention capacity, the lung accumulates NPs preferentially following ALI.[24] In treatment of inflammatory diseases, a passive targeting mechanism called ELVIS (extravasation through leaky vasculature and the subsequent sequestration by inflammatory cells) is beneficial to the targeting effect and tissue residence of NPs and is responsible for this preferential accumulation.[25,26] The size, shape, and surface charge of particles have been proven to be "standard" parameters that affect cellular interactions and uptake processes.[27] The deformability of nanoparticles has been considered an important feature affecting cell uptake. This study successfully synthesized flexible mesoporous silica particles bridged with sulfur ether, benzene, and ethane through preferential etching method, which can significantly improve cell internalization rate. In addition, the porous structure characteristics of HMONs can enhance drug loading and release performance.[28] Previous studies have shown that TMP can improve acute lung injury in mice. Therefore, TMP-loaded mesoporous silica NPs were prepared and characterized. Our results showed that mesoporous silica has a high specific surface area, uniform and adjustable pore size, good biocompatibility, extended retention time, and physiological stability. Glucocorticoids (such as dexamethasone), as strong anti-inflammatory drugs, are widely used to improve the clinical symptoms of ALI by limiting tissue damage and acute inflammatory reactions,[29–31] so they were used as a positive control in the experiment. NPs@TMP can reduce the level of inflammatory cytokines and inhibit lung oxidative stress in ALI mouse models in vitro. Histopathological studies also confirmed that NPs@TMP can reduce inflammation and lung injury.

We loaded the miR-194-5p in NPs@PEI and the expression of miR-194-5p was significantly increased in both cells and lung tissues. Thus, NPs@PEI@miR-194-5p can significantly inhibit the Rac1/ZO-1/Occludin pathway and improve the leakage of pulmonary capillary endothelial cells. In addition, compared to the NPs@TMP and NPs@PEI@miR-194-5p groups, NPs@TMP and NPs@PEI@MiR-194-5p combination therapy showed greater therapeutic effect in improving pulmonary inflammation, oxidative stress, and endothelial cell permeability. Moreover, the combination therapy significantly improved the survival rate of ALI. Histopathological studies revealed that NPs@TMP and NPs@PEI@miR-194-5p combination can better improve lung pathological damage. We believe that integrating multiple methods is a promising strategy to treat ALI. Traditional lung treatment drugs are distributed throughout the body after administration, and cannot be concentrated in lung tissue, which can cause damage to other organs. Given the urgent need for the treatment of devastating lung disease, it is our hope that these findings will encourage the development of new lung drug delivery systems based on HMONdds. These findings suggest that the effective release of the traditional Chinese medicine TMP and the newly identified miR-194-5p through the use of modified NPs could lead to the development of innovative therapeutic approaches for ALI. Next, we will further explore nanodrug delivery systems that can target lung tissue and deliver drugs efficiently. It is hoped that these findings will provide a novel understanding of ALI pathogenesis and a theoretical basis for ALI treatment.

Acknowledgments

This work was supported by the National Natural Science Foundation of China (81673791), Anhui Province Postgraduate Scientific Research Innovation Project (YJS20210528), Natural Science Climbing Program of Bengbu Medical College (2021bypd005), Key laboratory fund item of Anhui province (KLICD-2022-Z5), Provincial Graduate Innovation Practice Program (2022cxcysj170) and National University Students Innovation Training Program (202210367031, 202310367028).

Author Contributions

All authors made a significant contribution to the work reported, whether that is in the conception, study design, execution, acquisition of data, analysis and interpretation, or in all these areas; took part in drafting, revising or critically reviewing the article; gave final approval of the version to be published; have agreed on the journal to which the article has been submitted; and agree to be accountable for all aspects of the work.

Disclosure

This research was conducted without any commercial or financial relationships that could be construed as potential conflicts of interest.

References

1. Akyol A, Ulusoy H, Imamoğlu M, et al. Does propofol or caffeic acid phenethyl ester prevent lung injury after hindlimb ischaemia-reperfusion in ventilated rats? *Injury*. 2006;37(5):380–387. doi:10.1016/j.injury.2006.01.004
2. Kaukonen KM, Bailey M, Pilcher D, Cooper DJ, Bellomo R. Systemic inflammatory response syndrome criteria in defining severe sepsis. *N Engl J Med*. 2015;372(17):1629–1638. doi:10.1056/NEJMoa1415236
3. Khemani RG, Smith LS, Zimmerman JJ, Erickson S. Pediatric acute respiratory distress syndrome: definition, incidence, and epidemiology: proceedings from the pediatric acute lung injury consensus conference. *Pediatr Crit Care Med*. 2015;16(5 Suppl 1):S23–40. doi:10.1097/pcc.0000000000000432
4. Erlinger TP, Platz EA, Rifai N, Helzlsouer KJ. C-reactive protein and the risk of incident colorectal cancer. *JAMA*. 2004;291(5):585–590. doi:10.1001/jama.291.5.585
5. Huang X, Xiu H, Zhang S, Zhang G. The role of macrophages in the pathogenesis of ALI/ARDS. *Mediators Inflamm*. 2018;2018:1264913. doi:10.1155/2018/1264913
6. Ware LB, Matthay MA. The acute respiratory distress syndrome. *N Engl J Med*. 2000;342(18):1334–1349. doi:10.1056/nejm200005043421806
7. Odenwald MA, Choi W, Buckley A, et al. ZO-1 interactions with F-actin and occludin direct epithelial polarization and single lumen specification in 3D culture. *J Cell Sci*. 2017;130(1):243–259. doi:10.1242/jcs.188185
8. Cai L, Gao L, Zhang G, et al. DJ-1 alleviates neuroinflammation and the related blood-spinal cord barrier destruction by suppressing NLRP3 inflammasome activation via SOCS1/Rac1/ROS pathway in a rat model of traumatic spinal cord injury. *J Clin Med*. 2022;11(13):3716. doi:10.3390/jcm11133716
9. Rolland WB, Krafft PR, Lekic T, et al. Fingolimod confers neuroprotection through activation of Rac1 after experimental germinal matrix hemorrhage in rat pups. *J Neurochem*. 2017;140(5):776–786. doi:10.1111/jnc.13946
10. Yaoita E, Nishimura H, Nameta M, et al. Avian podocytes, which lack nephrin, use adherens junction proteins at intercellular junctions. *J Histochem Cytochem*. 2016;64(1):67–76. doi:10.1369/0022155415611708
11. Yang Y, Chen QH, Liu AR, Xu XP, Han JB, Qiu HB. Synergism of MSC-secreted HGF and VEGF in stabilising endothelial barrier function upon lipopolysaccharide stimulation via the Rac1 pathway. *Stem Cell Res Ther*. 2015;6(1):250. doi:10.1186/s13287-015-0257-0
12. Liu G, Bi Y, Wang R, et al. Kinase AKT1 negatively controls neutrophil recruitment and function in mice. *J Immunol*. 2013;191(5):2680–2690. doi:10.4049/jimmunol.1300736
13. Cao Y, Lyu YI, Tang J, Li Y. MicroRNAs: novel regulatory molecules in acute lung injury/acute respiratory distress syndrome. *Biomed Rep*. 2016;4(5):523–527. doi:10.3892/br.2016.620
14. Lefer AM, Lefer DJ. Pharmacology of the endothelium in ischemia-reperfusion and circulatory shock. *Annu Rev Pharmacol Toxicol*. 1993;33(1):71–90. doi:10.1146/annurev.pa.33.040193.000443
15. Dillioglugil MO, Kir HM, Demir C, et al. Effect of pentylenetetrazole and sound stimulation induced single and repeated convulsive seizures on the MDA, GSH and NO levels, and SOD activities in rat liver and kidney tissues. *Brain Res Bull*. 2010;83(6):356–359. doi:10.1016/j.brainresbull.2010.09.007
16. Mehla J, Reeta KH, Gupta P, Gupta YK. Protective effect of curcumin against seizures and cognitive impairment in a pentylenetetrazole-kindled epileptic rat model. *Life Sci*. 2010;87(19–22):596–603. doi:10.1016/j.lfs.2010.09.006
17. Horng CT, Huang JK, Wang HY, Huang CC, Chen FA. Antioxidant and antifatigue activities of polygonatum alte-lobatum hayata rhizomes in rats. *Nutrients*. 2014;6(11):5327–5337. doi:10.3390/nu6115327
18. Huang S, Lin H, Deng SG. Study of anti-fatigue effect in rats of ferrous chelates including hairtail protein hydrolysates. *Nutrients*. 2015;7(12):9860–9871. doi:10.3390/nu7125504
19. Teng Z, Wang C, Tang Y, et al. Deformable hollow periodic mesoporous organosilica nanocapsules for significantly improved cellular uptake. *J Am Chem Soc*. 2018;140(4):1385–1393. doi:10.1021/jacs.7b10694
20. Ben Djemaa S, Hervé-Aubert K, Lajoie L, et al. gH625 cell-penetrating peptide promotes the endosomal escape of nanovectorized siRNA in a triple-negative breast cancer cell line. *Biomacromolecules*. 2019;20(8):3076–3086. doi:10.1021/acs.biomac.9b00637
21. Stapleton PA, Minarchick VC, McCawley M, Knuckles TL, Nurkiewicz TR. Xenobiotic particle exposure and microvascular endpoints: a call to arms. *Microcirculation*. 2012;19(2):126–142. doi:10.1111/j.1549-8719.2011.00137.x
22. Tsai TH, Liang C. Pharmacokinetics of tetramethylpyrazine in rat blood and brain using microdialysis. *Int J Pharm*. 2001;216(1–2):61–66. doi:10.1016/s0378-5173(01)00572-5
23. Gao HJ, Liu PF, Li PW, et al. Ligustrazine monomer against cerebral ischemia/reperfusion injury. *Neural Regen Res*. 2015;10(5):832–840. doi:10.4103/1673-5374.156991
24. Hamadani CM, Goetz MJ, Mitragotri S, Tanner EEL. Protein-avoidant ionic liquid (PAIL)-coated nanoparticles to increase bloodstream circulation and drive biodistribution. *Sci Adv*. 2020;6(48). doi:10.1126/sciadv.abd7563

25. Tu Y, Lv M, Xiu P, et al. Destructive extraction of phospholipids from Escherichia coli membranes by graphene nanosheets. *Nat Nanotechnol*. 2013;8(8):594–601. doi:10.1038/nnano.2013.125
26. Song H, Ahmad Nor Y, Yu M, et al. Silica nanopollens enhance adhesion for long-term bacterial inhibition. *J Am Chem Soc*. 2016;138 (20):6455–6462. doi:10.1021/jacs.6b00243
27. Sun H, Wong EHH, Yan Y, et al. The role of capsule stiffness on cellular processing. *Chem Sci*. 2015;6(6):3505–3514. doi:10.1039/c5sc00416k
28. Min S, Tao W, Ding D, et al. Tetramethylpyrazine ameliorates acute lung injury by regulating the Rac1/LIMK1 signaling pathway. *Front Pharmacol Jan*. 2023;13:1005014. doi:10.3389/fphar.2022.1005014.29
29. Zhang Z, Chen L, Ni H. The effectiveness of Corticosteroids on mortality in patients with acute respiratory distress syndrome or acute lung injury: a secondary analysis. *Sci Rep*. 2015;5(1):17654. doi:10.1038/srep17654
30. Reis FF, Reboredo Mde M, Lucinda LM, et al. Pre-treatment with dexamethasone attenuates experimental ventilator-induced lung injury. *J Bras Pneumol*. 2016;42(3):166–173. doi:10.1590/s1806-37562015000000350
31. García-Fernández A, Sancho M, Bisbal V, et al. Targeted-lung delivery of dexamethasone using gated mesoporous silica nanoparticles. A new therapeutic approach for acute lung injury treatment. *J Control Release*. 2021;337:14–26. doi:10.1016/j.jconrel.2021.07.010